DETERMINATION OF DRAG AND LIFT RELATED COEFFICIENTS OF AN AUV USING COMPUTATIONAL AND EXPERIMENTAL FLUID DYNAMICS METHODS

(DOI No: 10.3940/rina.ijme.2020.a2.600)

E Javanmard, Sh Mansoorzadeh and **A Pishevar**, Isfahan University of Technology, Iran, and **J A Mehr**, University of Tasmania, Australia

SUMMARY

Determination of hydrodynamic coefficients is a vital part of predicting the dynamic behavior of an Autonomous Underwater Vehicle (AUV). The aim of the present study was to determine the drag and lift related hydrodynamic coefficients of a research AUV, using Computational and Experimental Fluid Dynamics methods. Experimental tests were carried out at AUV speed of 1.5 m s^{-1} for two general cases: I. AUV without control surfaces (Hull) at various angles of attack in order to calculate Hull related hydrodynamic coefficients and II. AUV with control surfaces at zero angle of attack but in different stern angles to calculate hydrodynamic coefficients related to control surfaces. All the experiments carried out in a towing tank were also simulated by a commercial computational fluid dynamics (CFD) code. The hydrodynamic coefficients obtained from the numerical simulations were in close agreement with those obtained from the experiments.

NOMENCLATURE

A_f	Hull frontal area (m^2)
A_{fl}	Hull longitudinal area (m^2)
a, b, c	Coefficients of second-order polynomial
b_{fin}	Fin span (m)
C_D	Drag force coefficient
C_L	Lift force coefficient
C_M	Moment coefficient
$C_{L\alpha}$	Hull Lift coefficient slop
$C_{M\alpha}$	Hull Moment coefficient slop
C_{Lf}	Fin lift coefficient
$C_{Lf_{\delta_e}}$	Rate of change of fin lift coefficient with respect to the effective fin angle
c_{root}	Fin root chord length (m)
c_{tip}	Fin tip chord length (m)
D	Drag force (N)
E	Comparison error
e_a^{21}	Approximate relative error
e_{ext}^{21}	Extrapolated relative error
d	Hull diameter (m)
K	Roll moment (N m)
L	Lift force (N)
L_{fin}	Fin lift force (N)
l	Hull length (m)
M	Pitch moment
$M_{fin\ st}$	Stern fin moment (N m)
N	Yaw moment (N m)
P	Pressure (N m^{-2})
p_a	Apparent order
P_{ref}	Reference pressure (N m^{-2})
p	Roll angular velocity (rad s^{-1})
q	Pitch angular velocity (rad s^{-1})
r	Yaw angular velocity (rad s^{-1})
r_o	Position vector of the vehicle with respect to the earth fixed frame
r_{ij}	Grid refinement factor of j^{th} grid toward i^{th} grid
Re_d	Reynolds based on diameter
Re_l	Reynolds based on length
s_{fin}	Fin Planform area (m^2)
u	Surge velocity(m s^{-1})
U_D	Experimental data uncertainty
U_I	Iterative uncertainty
U_G	Grid uncertainty
U_{TS}	Time step uncertainty
U_{SN}	Numerical simulation uncertainty
U_V	Validation uncertainty
V	Reference velocity (m s^{-1})
v	Sway velocity (m s^{-1})
v_e	Effective fin velocity (m s^{-1})
w	Heave velocity (m s^{-1})
X	Surge force (N)
x_{fin}	Axial position of the fin post in body-fixed coordinates or moment arm (m)
Y	Sway force (N)
Z	Heave force (N)
α	Angle of attack (degree)
δ_l	Boundary layer thickness (m)
δ_e	Effective fin angle (degree)
δ_{es}	Effective stern angle (degree)
δ_{er}	Effective rudder angle (degree)
δ_s	Stern angle (degree)
δ_r	Rudder angle (degree)
ρ	Density (kg m^{-3})
Δy	First layer thickness (m)
Δy^+	Dimensionless first layer thickness
$\emptyset$	Roll angle (degree)
θ	Pitch angle (degree)
ψ	Yaw angle (degree)
$\emptyset_{ext}^{21}$	Extrapolated value
AUV	Autonomous Underwater Vehicle
ASE	Analytical & Semi-Empirical
CFD	Computational Fluid Dynamics
CD	Conning Device
DOF	Degree of freedom
EFD	Experimental Fluid Dynamics
GCI	Grid Convergence Index

PMM	Planar Motion Mechanism
RANS	Reynolds-Averaged Navier-Stokes
RSM	Reynolds Stress Model
RSS	Root Sum of Square
SST	Shear Stress Transport
UUV	Unmanned Underwater Vehicle

1. INTRODUCTION

The hydrodynamic performance of autonomous unmanned underwater vehicles (UUV) is an area of interest with implications for control, navigation, launch and recovery, energy requirements and payload (Jones 2002). To investigate the hydrodynamic performance of UUVs, the dynamic governing equations, including three translational and three rotational equations must be solved. Since the forces and moments in these equations should be expressed in terms of hydrodynamic coefficients, these coefficients should be provided to the program as a priority. A number of methods have been developed for predicting the hydrodynamic coefficients of submersible vehicles including Computational Fluid Dynamics (CFD), Experimental Fluid Dynamics (EFD) and Analytical & Semi-Empirical (ASE) methods. Hopkin and Den Hertog (1993), Nahon (1993), Bellevre *et al*. (2000), Wu *et al*. (2005), Tyagi and Sen (2006), Phillips *et al*. (2007), Broglia *et al*. (2007), Barros *et al*. (2008), Sakamoto (2009), Tang *et al*. (2009), Jagadeesh and Murali (2010), Zhang *et al*.(2010), Phillips *et al*. (2010a, 2010b), Malik *et al*.(2013), Mansoorzadeh and Javanmard (2014), Leong *et al*. (2015), Kim *et al*. (2015), Liang *et al*. (2016), Pook *et al*. (2018), Javanmard and Mansoorzadeh (2019) are among those researchers who used computational fluid dynamics to obtain hydrodynamics coefficients.

Depending on the nature of hydrodynamic coefficients, which may be related to velocity, acceleration or rotation, various experimental facilities are required to estimate these coefficients. Towing tanks, Planar Motion Mechanisms (PMM), rotating arms and Coning Devices (CD) have been used by many researchers to experimentally obtain hydrodynamic coefficients. Gertler (1967), Aage *et al*. (1994), Rhee *et al*. (2001), Ridley *et al*. (2003), Jagadeesh *et al*. (2009), Lee *et al*. (2011), Avila *et al*., (2012), Javanmard (2013), Zhang and Zou (2013), Krishnankutty (2014), Saeidinezhad *et al*. (2015) and Kim *et al*. (2015) have used experimental methods for calculating hydrodynamic coefficients.

Peterson (1980), Humphreys (1981), Maeda and Tatsuta (1989), Nahon (1993) and Jones and Clarke (2002), on the other hand, have used ASE methods for calculating the hydrodynamic coefficients. While there are various methods used for the calculation of hydrodynamic coefficients, there are not many references in which the experimental, ASE and CFD results for the hydrodynamic coefficients are compared.

In this paper, both experimental and CFD methods are used to calculate velocity related hydrodynamic coefficients, for a research AUV shown in Figure 1. The main characteristics of the AUV are also specified in Table 1. The AUV is equipped with four identical control surfaces which have a NACA0015 cross-section. The specifications of the control surfaces are given in Table 2 and Figure 2. To conduct the experiments, a full-scale model of the AUV was tested in a towing tank with length, width and depth of the towing 108m, 3m and 2.2m, respectively. The experimental results were then compared with those obtained by CFD using a commercial code.

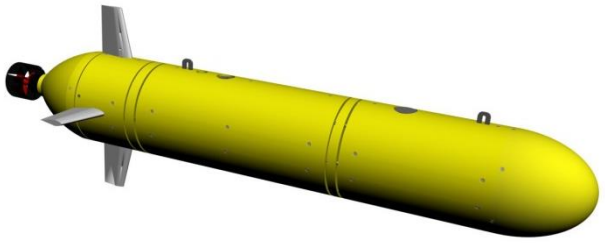

Figure 1: Autonomous Underwater Vehicle used in this study

Table 1: AUV Characteristics

Parameters	Description
Shape	Torpedo
Length (m)	1.45
Diameter (m)	0.23
Weight in air (kg)	45
Depth of operation (m)	2
Time of operation (hr)	2.5
Fin Profile	NACA0015
Horizontal velocity (Knot)	3

Table 2: Parameters of the Fins (NACA0015)

Parameter	s_{fin} (m^2)	b_{fin} (m)	x_{fin} (m)	c_{root} (m)	c_{tip} (m)
Value	0.009	0.12	-0.41	0.09	0.06

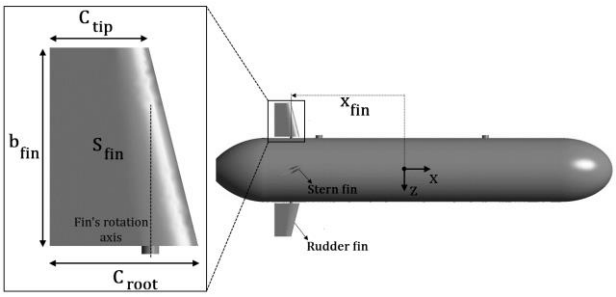

Figure 2: Schematic of the fin on the AUV

2. VEHICLE RIGID-BODY DYNAMICS

2.1 COORDINATE SYSTEM AND HYDRODYNAMIC LOADS

When modeling the motion of a submersible vehicle, it is convenient to introduce two reference frames, namely, earth-fixed and body-fixed reference frames. In the earth-fixed reference frame, the position and orientation of the vehicle are given relative to a fixed origin. The body fixed reference frame, on the other hand, is a moving coordinate frame fixed to the vehicle. Linear and angular velocities are given relative to this frame. The earth-fixed and body fixed coordinate frames for a 6-DOF vehicle motion are shown in Figure 3. The terms in the equation of motion which represent the hydrodynamic forces and moments acting on the vehicle are often expanded in a Taylor series about reference point.

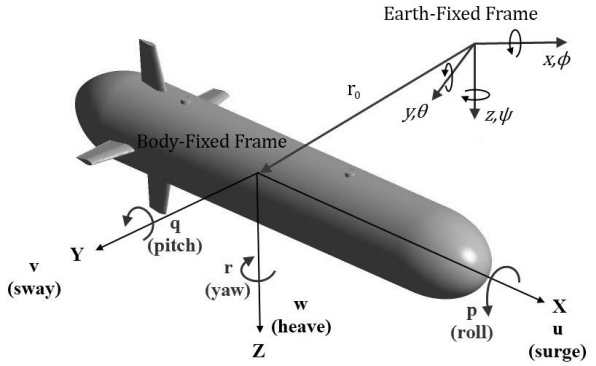

Figure 3: Forces and moments acting on the AUV in the earth and body fixed coordinate systems

The three components of hydrodynamic force along the x, y and z directions are denoted by X, Y and Z, respectively, and the three components of hydrodynamic moment about x, y and z are denoted by K, M and N. The three components of force and three components of moment are expanded to the second order terms in the linear velocities, u, v and w and linear angular velocity p, q and r. It is assumed that the sway velocity, v, and heave velocity, w, are small, compared to the surge velocity, u. By taking into account hydrostatic and added mass forces for an AUV, the external force and moment components can be expressed in terms of hydrodynamic coefficients, as shown in Equations 1-6 (Prestero, 2001).

$$\sum X_{net} = X_{HS} + X_{u|u|}u|u| + X_{w|w|}w|w| + X_{v|v|}v|v| + X_{\dot{u}}\dot{u} + X_{wq}wq + X_{qq}qq + X_{vr}vr + X_{rr}rr + X_{uv}uv + X_{u|w|}u|w| + X_{prop} \quad (1)$$

$$\sum Y_{net} = Y_{HS} + Y_{v|v|}v|v| + Y_{r|r|}r|r| + Y_{\dot{v}}\dot{v} + Y_{\dot{r}}\dot{r} + Y_{ur}ur + Y_{wp}wp + Y_{pq}pq + Y_{uv}uv + Y_{uu\delta_r}u^2\delta_r \quad (2)$$

$$\sum Z_{net} = Z_{HS} + Z_{w|w|}w|w| + Z_{q|q|}q|q| + Z_{\dot{w}}\dot{w} + Z_{\dot{q}}\dot{q} + Z_{uq}uq + Z_{vp}vp + Z_{rp}rp + Z_{uw}uw + Z_{uu\delta_r}u^2\delta_r \quad (3)$$

$$\sum K_{net} = K_{HS} + K_{P|P|}p|p| + K_P\dot{p} + K_{prop} \quad (4)$$

$$\sum M_{net} = M_{HS} + M_{w|w|}w|w| + M_{q|q|}q|q| + M_{\dot{w}}\dot{w} + M_{\dot{q}}\dot{q} + M_{uq}uq + M_{vp}vp + M_{rp}rp + M_{uw}uw + M_{uu\delta_s}u^2\delta_s \quad (5)$$

$$\sum N_{net} = N_{HS} + N_{v|v|}v|v| + N_{r|r|}r|r| + N_{\dot{v}}\dot{v} + N_{\dot{r}}\dot{r} + N_{ur}ur + N_{wp}wp + N_{pq}pq + N_{uv}uv + N_{uu\delta_r}u^2\delta_r \quad (6)$$

The hydrodynamic coefficients in these equations can be divided into three general groups: the coefficients related to the hydrostatic forces, which are denoted by subscript *HS*, the coefficients related to drag and lift forces and coefficients related to the added mass forces. In this paper, we are only dealing with coefficients related to the drag and lift forces. In Equations 1-6, the subscript notation represents the partial differentiation, e.g. $X_{u|u|} = \frac{\partial}{\partial u}\left(\frac{\partial X}{\partial u}\right)$ is the coefficient of $u|u|$ which is a drag related hydrodynamic coefficient, $Y_{uv} = \frac{\partial}{\partial u}\left(\frac{\partial Y}{\partial v}\right)$ is the coefficient of uv which is a body lift coefficient, $X_{\dot{u}} = \left(\frac{\partial X}{\partial \dot{u}}\right)$ is the coefficient of $\dot{u}$ which is an added mass coefficient in x direction. The terms containing δ_r and δ_S (the rudder and stern angles) are the hydrodynamic coefficients of control surfaces. X_{prop} and K_{prop} denote propeller thrust and propeller torque respectively. The rest of hydrodynamic coefficients in these equations can be explained in the same way. These equations explain how to calculate the forces and moments applied to an AUV by using the hydrodynamic coefficients. However, the method of calculating the hydrodynamic coefficients remains to be specified. Slender body theory is a reasonably accurate method for calculating added mass, but for viscous terms it can be off by as much as 100% (Triantafyllou, 2002).

The aim of the current paper is to present a CFD and experimental method to calculate the drag and lift related hydrodynamic coefficients appeared in Equations 1-6. The details of the procedure to calculate theses coefficients are explained in Section 2.2.

2.2 HYDRODYNAMIC COEFFICIENTS OF THE HULL

Figure 4 shows the drag and lift forces in the x-z plane acting on the AUV without control surfaces (Hull). Drag and lift act parallel and perpendicular to the flow, respectively.

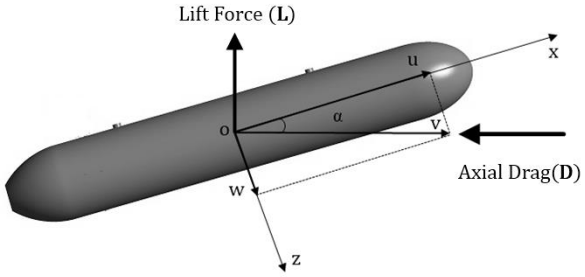

Figure 4: Drag and lift forces in the x-z plane acting on the hull

These forces can be resolved in the x-z plane to obtain X and Z components of the force as follows:

$$X = L\sin\alpha - D\cos\alpha \quad (7)$$
$$Z = -L\cos\alpha - D\sin\alpha \quad (8)$$

Where L and D, are the lift and drag forces respectively. By assuming that the angle of attack α is small, the following approximations can be made:

$$\sin\alpha \approx \tan\alpha = \alpha = w/u \quad (9)$$
$$\cos\alpha \approx 1 - \alpha^2/2 \quad (10)$$
$$X = L\alpha - D(1 - \alpha^2/2) \quad (11)$$
$$Z = -L(1 - \alpha^2/2) - D\alpha \quad (12)$$

The drag and lift forces and the moment caused by the lift force can be calculated from the following equations (Hoerner, 1965 and 1985):

$$D = \frac{1}{2}\rho C_D A_f V^2 \quad (13)$$
$$L = \frac{1}{2}\rho C_L A_{fl} V^2 = \frac{1}{2}\rho C_{L\alpha}\alpha A_{fl} V^2 \quad (14)$$
$$M = \frac{1}{2}\rho C_M A_{fl} V^2 = \frac{1}{2}\rho C_{M\alpha}\alpha A_{fl} V^2 \quad (15)$$

Where ρ and V are the fluid density and velocity, respectively. A_f and A_{fl} are the frontal and longitudinal areas of the hull which are 0.0415 m^2 and 0.31494 m^2, respectively. C_D, C_L and C_M are the drag, lift and moment coefficients, respectively and $C_{L\alpha}$ and $C_{M\alpha}$ are the lift and moment slopes, respectively expressed as (Hoerner, 1985):

$$C_L = \frac{\partial C_L}{\partial \alpha}\alpha = C_{L\alpha}\alpha \quad (16)$$
$$C_M = \frac{\partial C_M}{\partial \alpha}\alpha = C_{M\alpha}\alpha \quad (17)$$

Assuming that the drag coefficient is a function of angle of attack, we can approximate it with a second-order polynomial as:

$$C_D(\alpha) = a\alpha^2 + b\alpha + c \quad (18)$$

And by writing the velocity vector in terms of its components in x-z plane, $V^2 = u^2 + w^2$, Equations 9-15 can be combined to obtain forces X, Z and moment M as follows:

$$\begin{aligned} X &= L\alpha - D(1 - \alpha^2/2) \\ &= \tfrac{1}{2}\rho C_{L\alpha} A_{fl}(u^2 + w^2).\alpha^2 \\ &-\tfrac{1}{2}\rho C_D A_f (u^2 + w^2)(1 - \alpha^2/2) \\ &\approx \tfrac{1}{2}\rho C_{L\alpha} A_{fl} w^2 - \tfrac{1}{2}\rho A_f\{(a + c/2)w^2 + buw + cu^2\} \end{aligned} \quad (19)$$

$$\begin{aligned} Z &= -L\cos\alpha - D\sin\alpha \\ &= -\tfrac{1}{2}\rho C_{L\alpha}\alpha A_{fl}\,(u^2 + w^2)(1 - \alpha^2/2) \\ &-\tfrac{1}{2}\rho C_D A_f (u^2 + w^2) \approx -\tfrac{1}{2}\rho C_{L\alpha} A_{fl} uw \\ &-\tfrac{1}{2}\rho A_f\{bw^2 + cuw\} \end{aligned} \quad (20)$$

$$\begin{aligned} M &= \frac{1}{2}\rho C_M A_{fl}(u^2 + w^2) \\ &= \tfrac{1}{2}\rho C_{M\alpha} A_{fl}(u^2 + w^2)\alpha \approx \tfrac{1}{2}\rho C_{M\alpha} A_{fl} uw \end{aligned} \quad (21)$$

To derive the above equations, the third and higher order terms are assumed to be negligible. By comparing the above equations with Equations 1-6, the following hydrodynamic coefficients can be derived.

$$X_{uu} = -\tfrac{1}{2}\rho A_f c \quad (22)$$
$$X_{ww} = -\tfrac{1}{2}\rho A_f (a + c/2) + \tfrac{1}{2}\rho C_{L\alpha} A_{fl} \quad (23)$$
$$X_{uw} = -\tfrac{1}{2}\rho A_f b \quad (24)$$
$$Z_{ww} = -\tfrac{1}{2}\rho A_f b \quad (25)$$
$$Z_{uw} = -\tfrac{1}{2}\rho A_f c - \tfrac{1}{2}\rho C_{L\alpha} A_{fl} \quad (26)$$
$$M_{uw} = \tfrac{1}{2}\rho C_{M\alpha} A_{fl} \quad (27)$$

Since the geometry of the AUV is symmetric with respect to the x-z and x-y planes, the hydrodynamic coefficients related to the x-y plane can be obtained as:

$$X_{ww} = X_{vv} \quad X_{uw} = X_{uv}$$
$$Z_{uw} = -Y_{uv} \quad N_{uv} = M_{uw} \quad Z_{ww} = -Y_{vv} \quad (28)$$

To calculate the hydrodynamic coefficients expressed in Equations 22-28, the variation of drag coefficient in terms of angle of attack must be known. In the present work, both experimental and numerical methods were used to determine the drag coefficients for various angles of attack. By fitting a second order polynomial on the obtained results, as expressed in Equation 18, coefficients a, b and c were determined.

To complete the calculation of hydrodynamic coefficients, as expressed in Equations 22-27, two other unknowns, namely, slope of the lift and moment coefficients, $C_{L\alpha}$ and $C_{M\alpha}$, need to be calculated. Again, both experimental and numerical methods were used to calculate theses parameters. To determine $C_{L\alpha}$, the lift force need to be first calculated experimentally or numerically, for different angles of attack. Then, the lift coefficient for every angle of attack should be calculated, using Equation 14. Plotting the variation of the lift force coefficient with angle of attack and calculating its slope, as shown in Equation 16, determined the coefficient $C_{L\alpha}$. This value could be replaced into Equations 23 and 26 to obtain the required hydrodynamic coefficients. The same procedure should be followed for calculation of $C_{M\alpha}$ and its associated hydrodynamic coefficients.

2.3 HYDRODYNAMIC COEFFICIENT OF THE CONTROL SURFACES

The altitude of the AUV vehicle is controlled by two horizontal fins, or stern fins, and two vertical fins, or rudders. As shown in Figure 5, a positive stern angle causes a negative fin lift force and a negative stern fin moment according to the defined body-fixed frame. The Lift force and the moment of the stern fins, which are designed to move together, can be calculated from the following equations:

$$L_{fin} = -\frac{1}{2}\rho C_{Lf_{\delta_e}} s_{fin} {v_e}^2 \delta_e \quad (29)$$

$$M_{fin\ st} = -x_{fin} L_{fin} \qquad (x_{fin} < 0) \quad (30)$$

Where, L_{fin} is the fin lift force, s_{fin} is the control fin planform area, v_e is effective fin velocity, $C_{Lf_{\delta_e}} = \frac{\partial C_{lf}}{\partial \delta_e}$ is the rate of change of the lift coefficient C_{Lf} with respect to the effective fin angle δ_e. Effective fin angle can be defined for the rudder and stern fins as:

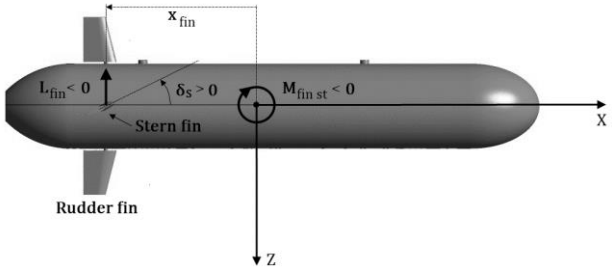

Figure 5: Lift force and the pitch moment in the x-z plane acting on the vehicle body

$$\delta_{es} = \delta_s + \frac{1}{u}(w - x_{fin} q) \quad (31)$$

$$\delta_{er} = \delta_r + \frac{1}{u}(w - x_{fin} r) \quad (32)$$

where x_{fin} is the fin distance from the body-fixed coordinate system. For small angle of attack; $v_e \approx u$. Substituting δ_e and v_e in Equation 29, using the definition of the hydrodynamic coefficient as described in the previous section and considering the symmetry condition in x-z and y-z planes, the following equations can be derived for the hydrodynamic coefficients related to the rudder and stern control surfaces (Ridley, 2001).

$$Y_{uu\delta_r} = -Y_{uvf} = \rho C_{Lf_{\delta_{es}}} s_{fin} \quad (33)$$

$$Z_{uu\delta_s} = Z_{uwf} = -\rho C_{Lf_{\delta_{es}}} s_{fin} \quad (34)$$

$$Y_{urf} = -Z_{uqf} = -\rho C_{Lf_{\delta_{es}}} s_{fin} x_{fin} \quad (35)$$

$$M_{uu\delta_s} = M_{uwf} = \rho C_{Lf_{\delta_{es}}} s_{fin} x_{fin} \quad (36)$$

$$N_{uu\delta_r} = -N_{uvf} = \rho C_{Lf_{\delta_{es}}} s_{fin} x_{fin} \quad (37)$$

$$N_{urf} = M_{uqf} = -\rho C_{Lf_{\delta_{es}}} s_{fin} {x_{fin}}^2 \quad (38)$$

To calculate the control surface hydrodynamic coefficients, both experimental and numerical methods were applied in the present work. For a zero angle of attack, α, the fin lift force was first calculated for various rudder or stern angles, δ_e. The fin lift coefficient was obtained using:

$$C_{Lf} = \frac{L_{fin}}{\frac{1}{2}\rho S_{fin} v_e^2} \quad (39)$$

The fin lift coefficient was then plotted against the fin angle δ_e. The slope of the curve $C_{Lf_{\delta_e}}$ could be introduced into Equations 33-38 to obtain the fin hydrodynamic coefficients. In the following sections, the experimental setup and numerical approach used for the calculation of hydrodynamic coefficients are explained.

3. EXPERIMENTAL SETUP

A full-scale model of the AUV was fabricated to conduct the experiments. The experiments were carried out in a towing tank with length, width and depth of 108m, 3m and 2.2m, respectively. The AUV model, as shown in Figure 6, was connected to the carriage dynamometer through two NACA0012 struts. The distance between the free surface and top of the AUV model was 60 cm. Table 3 shows the various parameters in which experiments were carried out. In order to measure the net force exerted on the vehicle body, experiments were carried out in two steps. In the first step, the force required to tow the AUV model together with struts at a specified speed was measured. In the second step, the forces required to tow only the struts in the same speed was measured. By subtracting the force measured in the first from the one in the second step, the net force required to tow only the vehicle body could be calculated.

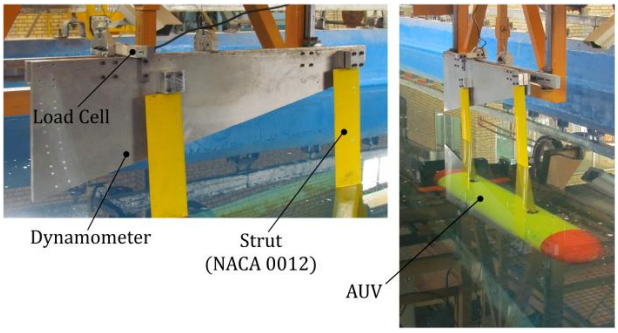

Figure 6: Experimental setup, indicating AUV model, the struts, dynamometer and load cell

Table 3: Experimental and numerical conditions

Cases	Model	V (m s^{-1})	α (degree)	δ_s (degree)
I	Hull	1.5	0,3,6,8,12,16	-
II	Hull + Fins	1.5	0	-8,-6,-4,-2, 0,2,4,6,8, 12,16

3.1 EXPERIMENTAL UNCERTAINTY ANALYSES

An uncertainty analysis with 95% confidence level was performed for hydrodynamic coefficients (C_D, C_L and C_M) calculated for two cases of the experiments: Case I with $\alpha = 16^o$ and Case II with $\delta_s = 16^o$. According to procedure proposed by Coleman and Steele (1999) and ITTC (2002), total uncertainty in calculated values of C_D, C_L and C_M is equal to Root Sum of Square (RSS) of bias errors (systematic uncertainty) and precision error (random uncertainty). For these coefficients, bias error was calculated as RSS of each elementary error including velocity, reference area, and density, calibration of the load cell, misalignment, data acquisition, data reduction, curve fitting as well as towing tank inclination. Precision error was obtained by repeating the experiments for five times using the standard deviation. Calculated values of C_D, C_L and C_M along with estimated experimental uncertainties (U_D) are given in Table 4.

Table 4: Experimental uncertainty analysis

Cases	Variables	Experimental Value	U_D(%)
Case I $\alpha = 16^o$	C_D	0.2478	6.1
	C_L	0.03533	5.72
	C_M	0.07737	5.88
Case II $\delta_s = 16^o$	C_D	0.2681	5.13
	C_L	0.0555	4.84
	C_M	-0.0312	4.97

4. NUMERICAL SIMULATIONS

The Reynolds-Averaged Navier–Stokes (RANS) governing equations that can model the flow field around the AUV are expressed in Equations 40 and 41 (White, 1985).

$$\frac{\partial \bar{U}_i}{\partial x_i} = 0 \tag{40}$$

$$\frac{\partial \bar{U}_i}{\partial t} + \frac{\partial \overline{U_i U_j}}{\partial x_j} = -\frac{1}{\rho}\frac{\partial p}{\partial x_i} + \frac{\partial}{\partial x_j}\left\{\upsilon\left(\frac{\partial \bar{U}_i}{\partial x_j} + \frac{\partial \bar{U}_j}{\partial x_i}\right)\right\} - \frac{\partial \overline{\acute{U}_i \acute{U}_j}}{\partial x_j} + f_i \tag{41}$$

To solve these equations, a commercial CFD code was used. The Shear Stress Transport (SST) turbulence model was implemented to model the Reynolds stress term, $\overline{\acute{U}_i \acute{U}_j}$, when the control surfaces were simulated and flow separation was important. SST is a two zone model which blends a variant of $k-\omega$ model with a $k-\varepsilon$ in the outer boundary layer and far from the wall. A $k-\varepsilon$ turbulence model was used when the hull body alone was calculated. The computational domain was a fixed cuboid in space and the solid body was a full-scale of the AUV positioned in various angles of attack as shown in Table 3. The inlet boundary condition was applied at 1.5 body length upstream of the model with various inflow velocities as indicated in Table 3. An outlet boundary condition with zero relative pressure defined at 3.5 body length downstream of the model. The boundary conditions for the side walls, located 6 diameters away from the AUV, were considered to be free-slip wall. No slip boundary condition was applied to the hull, as can be seen in Figure 7. ANSYS ICEM CFD was used to generate unstructured mesh, as shown in Figure 8. A finer mesh was used near large gradient areas, like control surfaces and the nose of the AUV. A prism layer near the wall of quadrilateral cells was generated to resolve the high gradient boundary layer. For a specified y^+, the first layer thickness can be estimated as (ANSYS CFX Release 12.1, 2009):

$$\Delta y = l\Delta y^+ \sqrt{80}\, Re_l^{-\frac{13}{14}} \tag{42}$$

and the boundary layer thickness δ_l can be obtained using (White, 2006):

$$\frac{\delta_l}{l} = \frac{0.382}{Re_l^{0.2}} \tag{43}$$

For a velocity of 1.5 m s^{-1} and a $y^+ = 30$ for $k-\varepsilon$ turbulence model, the first layer thickness and the boundary layer thickness were about 0.5105 mm and 29 mm, respectively. Therefore, by using an expansion factor of 1.3, the boundary layer would contain 13 layers of meshes. In order to obtain the required hydrodynamic coefficients, simulations were carried out for a variety of cases shown in Table 3.

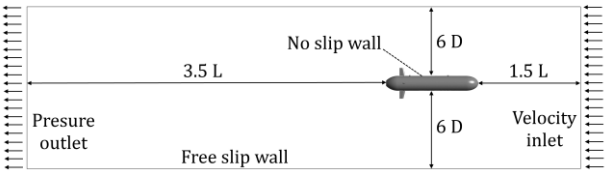

Figure 7: Boundary conditions in numerical simulations

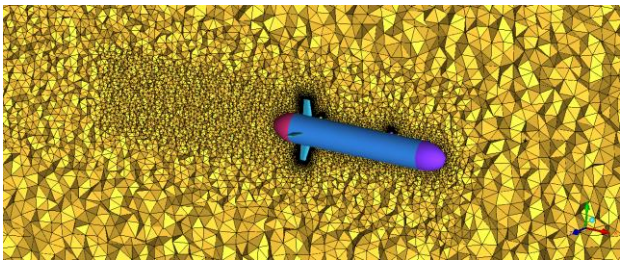

Figure 8: Unstructured mesh in computational domain

4.1 GRID INDEPENDENCE STUDY

To perform a grid independence study, for each general case of simulations three grid configurations classified as coarse, medium and fine were generated with a systematic grid refinement of $\sqrt{2}$ at the most critical position of each case, $\alpha = 16^o$ for Case I and $\delta_s = 16^o$ for Case II. The specifications of the studied grids are shown in Table 5. For each mesh configuration, drag coefficient (C_D) was computed at V=1.5 m s^{-1} that is also given in Table 5. Clearly, the fine-mesh configurations have the minimum relative differences from the experimental data. Therefore, using fine-mesh configuration for each case, ensured that the results were grid independent and numerically cost effective.

Table 5: C_D results at three grid resolutions and Comparison error (E) between numerical and experimental data

Case I, $\alpha = 16^o$			
Mesh Configuration	Coarse	Medium	Fine
Number of Elements	1.4×10^6	3.01×10^6	6.1×10^6
C_D (CFD)	0.2090	0.2299	0.2375
C_D (EFD)	0.2478	0.2478	0.2478
E (%)	15.66	7.22	4.16
Case II, $\delta_s = 16^o$			
Mesh Configuration	Coarse	Medium	Fine
Number of Elements	2.12×10^6	4.3×10^6	8.75×10^6
C_D (CFD)	0.2311	0.2503	0.2590
C_D (EFD)	0.2681	0.2681	0.2681
E (%)	13.8	6.64	3.39

4.2 VERIFICATION AND VALIDATION STUDY

To assess the capability of the proposed CFD model in solving the system of equations, when adequately fine grid resolution is employed, the Grid Convergence Index (GCI) method was applied. This method is based on Richardson extrapolation method (Richardson, 1911; Richardson and Gant, 1927) and is a recommended method for estimation of discretization error in CFD simulations (Ferziger and Peric, 2002; Celik *et al*., 2008).

The apparent order of the method, p_a, is calculated by:

$$p_a = |\ln|\varepsilon_{32}/\varepsilon_{21}| + q(p_a)|/\ln(r_{21}) \quad (44)$$

$$q(p_a) = \ln\{(r_{21}^{p_a} - s)/(r_{32}^{p_a} - s)\} \quad (45)$$

$$s = 1.\ sign(\varepsilon_{32}/\varepsilon_{21}) \quad (46)$$

Where r_{21} and r_{32} are refinement factors, i.e. $\sqrt{2}$ in this work, and $\varepsilon_{32} = \emptyset_3 - \emptyset_2$, $\varepsilon_{21} = \emptyset_2 - \emptyset_1$ that $\emptyset_k$ is the key variable, i.e. C_d in this study, on the k^{th} grid. The extrapolated values are obtained via:

$$\emptyset_{ext}^{21} = (r_{21}^{p_a}\emptyset_1 - \emptyset_2)/(r_{21}^{p_a} - 1) \quad (47)$$

The approximate and extrapolated relative errors are calculated using the following equations, respectively.

$$e_a^{21} = |(\emptyset_1 - \emptyset_2)/\emptyset_1| \quad (48)$$

$$e_{ext}^{21} = |(\emptyset_{ext}^{21} - \emptyset_1)/\emptyset_{ext}^{21}| \quad (49)$$

The fine-grid convergence index is calculated by:

$$GCI_{fine}^{21} = 1.25e_a^{21}/(r_{21}^{p_a} - 1) \quad (50)$$

In fact the GCI verification method estimates grid uncertainty (U_G) as one of the main sources of the numerical simulation uncertainty (U_{SN}). According to Equation 51, although iterative and time step uncertainties (U_I,U_{TS}) are other sources of numerical uncertainty (ITTC, 2017), grid uncertainty is regarded as the most important source of uncertainty of the numerical results (Wilson *et al*., 2001; ITTC, 2011). Therefore, the assumption of $U_{SN} \approx U_G$ was used in this study.

$$U_{SN}^2 = U_I^2 + U_G^2 + U_{TS}^2 \quad (51)$$

For three mesh configurations used for grid independence study, represented in Table 5, calculated numerical uncertainties of computed values of C_D, C_L and C_M are presented in Table 6. As can be seen, maximum numerical uncertainties are about 3.88% and 3.80% for computed values of C_L, for Case I with $\alpha = 16^o$, and C_M, for Case II with $\delta_s = 16^o$, respectively.

Using experimental and numerical results calculated for C_D, C_L and C_M besides estimated values of experimental and numerical uncertainties, comparison error (E) between experimental and numerical results as well as validation uncertainty (U_V) were calculated as shown in Table 7. It is worth mentioning that according to ITTC (2017), validation uncertainty (U_V) is given by

$$U_V^2 = U_{SN}^2 + U_D^2 \quad (52)$$

As can be seen in Table 7, obtained results for Case II ($\delta_s = 16^o$) show a good agreement between the experimental and the numerical results. In this case, the maximum comparison error was about 4.49%. Additionally, for all variables comparison error was

Table 6: Calculation of the discretization errors for C_D, C_L and C_M values

Cases	Variables	r_{21}, r_{32}	$\emptyset_1$	$\emptyset_2$	$\emptyset_3$	p_a	$\emptyset_{ext}^{21}$	e_a^{21}	e_{ext}^{21}	GCI_{fine}^{21}
Case I $\alpha = 16^o$	C_D	$\sqrt{2}$	0.2375	0.2299	0.2090	2.9189	0.2418	3.2%	1.778%	2.286%
	C_L	$\sqrt{2}$	0.0321	0.0308	0.0277	2.5075	0.0330	4.05%	2.842%	3.656%
	C_M	$\sqrt{2}$	0.0703	0.0672	0.0597	2.5492	0.0724	4.41%	3.013%	3.884%
Case II $\delta_s = 16^o$	C_D	$\sqrt{2}$	0.2590	0.2503	0.2311	2.2840	0.2662	3.36%	2.705%	3.48%
	C_L	$\sqrt{2}$	0.0531	0.0509	0.0457	2.4820	0.0547	4.14%	2.948%	3.798%
	C_M	$\sqrt{2}$	-0.0298	-0.0285	-0.0253	2.6107	-0.3068	4.35%	2.873%	3.697%

Table 7: Calculation of the comparison error (E) and validation uncertainty (U_V) for C_D, C_L and C_M values

Cases	Variables	EFD	CFD	U_D(%)	U_{SN}(%)	U_V(%)	Δ (%)
Case I $\alpha = 16^o$	C_D	0.2478	0.2375	6.1	2.286	6.514	4.156
	C_L	0.03533	0.0321	5.72	3.656	6.789	9.142
	C_M	0.07737	0.0703	5.88	3.884	7.047	9.138
Case II $\delta_s = 16^o$	C_D	0.2681	0.2590	5.13	3.48	6.199	3.394
	C_L	0.0555	0.0531	4.84	3.798	6.152	4.324
	C_M	-0.0312	-0.0298	4.97	3.697	6.194	4.487

smaller than validation uncertainty meaning that the combination of all the errors in EFD and CFD is smaller than U_V and validation was achieved at the validation uncertainty level (ITTC, 2017). On the other hand, obtained results for Case I ($\alpha = 16^o$) indicated that for C_D validation was also achieved since, in this case, comparison error is small (E =4.156%) and $E < U_V$. However, for C_L and C_M comparison error was around 9.1% and $E > U_V$. On the condition that the comparison error was much higher than validation uncertainty ($E \gg U_V$), the validation would not be achieved and the improvement of the numerical modeling might be taken into consideration.

Since in Case I, $\alpha = 16^o$ is the highest angle of attack in the current study, it is expected that at other angles of attack (0^o, 3^o, 6^o, 8^o and 12^o) with decreasing comparison error, the level of validation is improved. Obtained CFD results for C_L and C_M in other angles of attack demonstrated that there were significant improvements in validation level due to decreasing of the comparison error as indicated in the next section.

5. RESULTS AND DISCUSSION

As shown in Table 3, various sets of parameters have been used in our numerical and experimental investigations.

The results were obtained at different angles of attack, for the AUV with and without control surfaces. The results obtained by the two methods are presented below.

5.1 EXPERIMENTAL AND NUMERICAL RESULTS FOR HULL WITH ANGLES OF ATTACK (CASE I)

In order to calculate the drag and lift related hydrodynamic coefficients of the hull, using Equations 22-27, coefficients *a, b, c*, $C_{L\alpha}$ and $C_{M\alpha}$ should be known. Drag coefficient as a function of the angle of attack for a velocity of 1.5 m s^{-1} was obtained, both experimentally and numerically. Figure 9 compares the experimental and numerical results obtained for the variation of drag coefficient with the angle of attack for the hull alone. As illustrated in this figure, both experimental and numerical results showed that from $\alpha = 0^o$ to $\alpha = 6^o$ the drag coefficient was increased gradually and then from $\alpha = 6^o$ to $\alpha = 16^o$ it increased dramatically. To calculate *a, b* and *c,* as described in Section 2.2, a second order polynomial should be fitted to the numerical and experimental results, shown in Figure 9, as:

$$C_{D\,CFD}(\alpha) = 1.5581\alpha^2 - 0.1583\alpha + 0.159 \quad (53)$$
$$C_{D\,EFD}(\alpha) = 1.5451\alpha^2 - 0.1553\alpha + 0.1685 \quad (54)$$

Comparing Equations 53 and 54 with Equation 18, coefficients *a*, *b* and *c*, can be determined. To calculate $C_{L\alpha}$ and $C_{M\alpha}$, lift and moment coefficients of the hull (C_L and C_M) at various angles of attack were obtained experimentally and numerically as illustrated in Figures 10 and 11 respectively. The slope of these curves indicates $C_{L\alpha}$ and $C_{M\alpha}$ respectively. All these coefficients are presented in Table 8. The results obtained for *a, b, c*, $C_{L\alpha}$ and $C_{M\alpha}$ were used to calculate the drag and lift related hydrodynamic coefficients. Table 9 compares the numerical and

experimental results obtained for the hydrodynamic coefficients. According to Figures 9, 10 and 11, there are differences between experimental and numerical results. In other words, the experimental results are greater than their corresponding numerical values. This can be explained on the basis of the differences between the numerical and experimental conditions.

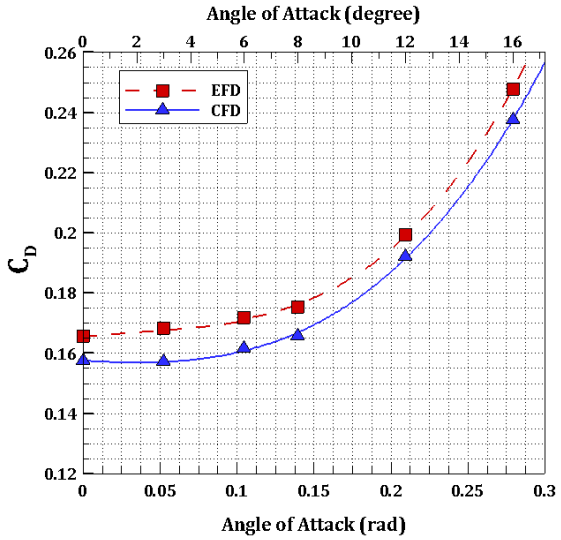

Figure 9: Variation of the drag coefficient of the hull with the angle of attack

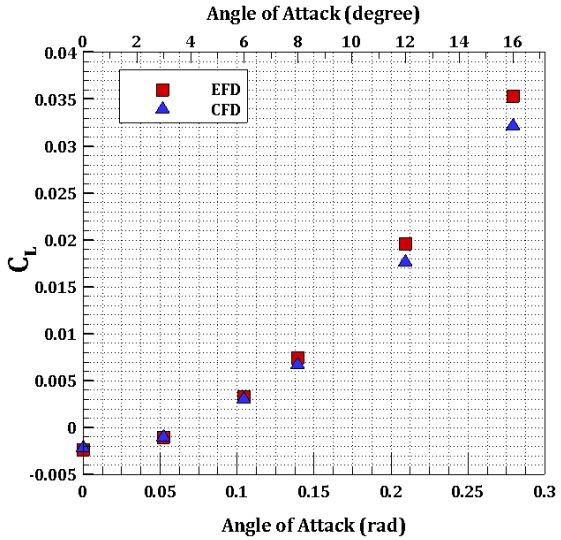

Figure 10: Variation of the lift coefficient of the hull with the angle of attack

Firstly, the numerical simulations were conducted in an infinite medium, while the experiments were carried out in a specific depth, i.e. the model of the AUV was located 60 cm below the water surface. Secondly, the interaction of the body with the surface wave and the reflected waves from the towing tank walls can increase the model motion resistance, hence the drag, lift and moment coefficients. This effect can be avoided by increasing the length of the struts. However, by increasing the length of struts, vibration and deflection of struts may cause more serious problems. Finally, the presence of struts in the experiments disturbs the fluid flow around the vehicle body and increases the resistance force. This effect does not exist in the numerical simulations. The effects of struts and free surface and their mutual interactions were investigated previously by Mansoorzadeh and Javanmard (2014) and Javanmard and Mansoorzadeh (2019). The results obtained from these researches indicated that at the AUV speed of 1.5 m s^{-1}, the assumption of infinite medium in numerical simulations caused a reduction of 2.11% in AUV drag predictions, in comparison with the numerical simulations performed in a two phase flow condition with a submergence depth of 60 cm.

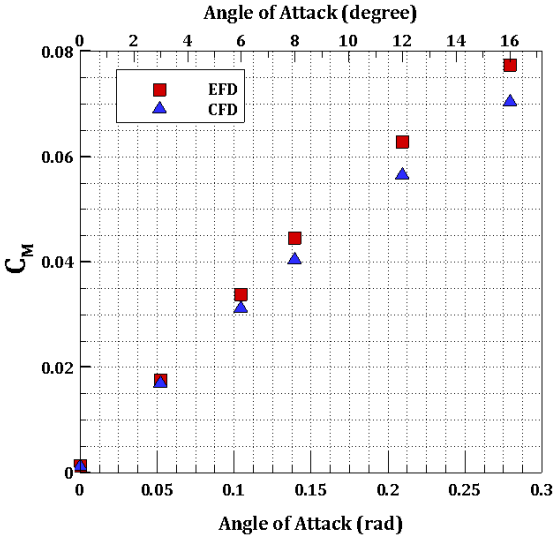

Figure 11: Variation of the moment coefficient of the hull with the angle of attack

Table 8: Derived coefficients of the hull

	a (rad^{-2})	b (rad^{-1})	c -	$C_{L\alpha}$ (rad^{-1})	$C_{M\alpha}$ (rad^{-1})
CFD	1.5581	-0.1583	0.159	0.1245	0.2474
EFD	1.5451	-0.1553	0.1685	0.1371	0.2752

Table 9: Numerical and experimental results for the drag and lift related hydrodynamic coefficients of the Hull

Hydrodynamic Coefficients	CFD	EFD	Units	E (%)
X_{uu}	-3.29	-3.49	kg m^{-1}	5.73
X_{ww}	-14.37	-12.22	kg m^{-1}	-17.59
X_{uw}	3.28	3.22	kg m^{-1}	-1.86
X_{vv}	-14.37	-12.22	kg m^{-1}	-17.59
X_{uv}	3.28	3.22	kg m^{-1}	-1.86
Y_{uv}	22.84	25.01	kg m^{-1}	8.68
Y_{vv}	-3.28	-3.22	kg m^{-1}	-1.86
Z_{ww}	3.28	3.22	kg m^{-1}	-1.86
Z_{uw}	-22.84	-25.01	kg m^{-1}	8.68
M_{uw}	38.84	43.21	kg	10.1
N_{uv}	38.84	43.21	kg	10.1

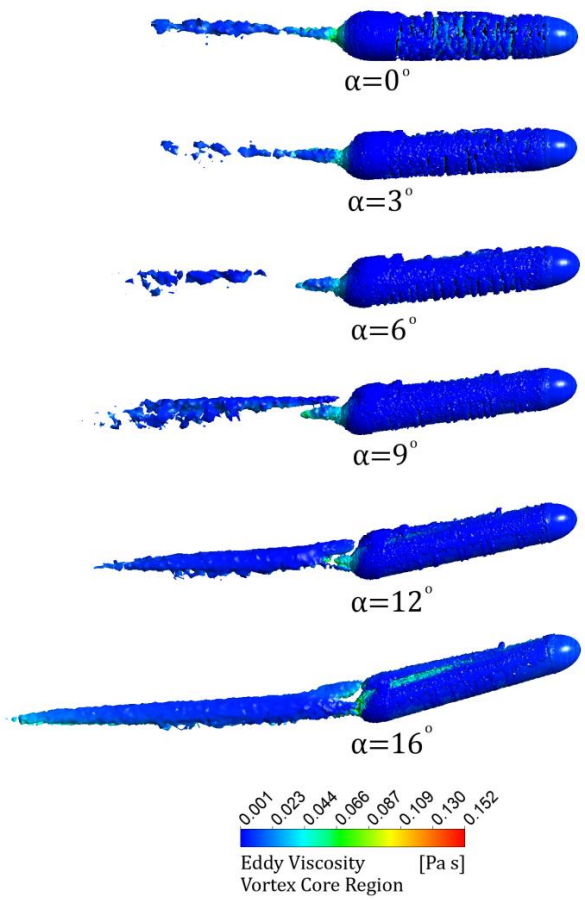

Figure 12: Eddy viscosity distribution on the vortex structures behind the hull at various angles of attack

On the other hand, the discrepancies between numerical and experimental values can be attributed to the accuracy of the applied turbulence model in capturing the strength and path of the crossflow induced body vortices encountered by the hull at an angle of attack. This is due to the modification of the pressure field around the body by the strength and location of the body vortex and this modification has a significant influence on the global forces and moments acting on the body (Phillips *et al*., 2010b). According to Chesnakas and Simpson (1997) and Phillips *et al*. (2010b), for a hull operating at a moderate drift angle the turbulence is anisotropic in the vortex sheets therefore employing eddy viscosity based turbulence methods such as $k-\varepsilon$ using the Boussinesq assumption to model Reynolds stresses leads to inaccurate numerical predictions for the hull. In this case, Reynolds Stress Model (RSM) has been recommended since the Reynolds stresses are derived directly from six transport equations. According to Figures 10 and 11, it is clear that discrepancy between numerical and experimental values increases at the higher angles of attack. The most important reason may be the weakness of the $k-\varepsilon$ model in predicting the strength and location of the body vortex at the higher angles of attack. This is the main reason why in Case I ($\alpha = 16^{o}$) validation level for C_L and C_M was low ($E > U_V$). Therefore, according to ITTC (2017), the improvement of the numerical modeling may reduce the comparison error and, in turn, increase the level of validation at the high angles of attack. In this case, a Reynolds Stress Model can be used to improve the numerical modeling and reduce the comparison error between the numerical and experimental results.

Figure 12 shows eddy viscosity distribution on the vortex structures behind the hull in various angles of attack. As shown, the vortex core structure behind the hull grew as the angle of attack increased, causing an increase in the drag force.

5.2 EXPERIMENTAL AND NUMERICAL RESULTS FOR THE CONTROL SURFACES (CASE II)

In the present study, experimental and numerical simulations were carried out to calculate the fin lift force at various stern angles, for a forward velocity of 1.5 m/s. Other components of linear and angular velocity were assumed to be zero. So, $w = q = 0$ and according to Equation 31, $\delta_{es} = \delta_s$. The fin lift coefficients were determined for each stern angle using Equation 39 and then were plotted against the stern angle, as shown in Figure 13. The slope of the curves, indicated in Table 10, could be introduced into Equations 33-38 to obtain the fin hydrodynamic coefficients. It should be noted that the numerical and experimental results obtained for the fin lift slope could be compared with the corresponding value given by Hoerner (1985) correlation for a NACA0015 presented in Table 10. Due to the symmetry of the AUV, the magnitude of the hydrodynamic coefficients of the rudder fins were equal to those of the sterns, and only the direction and sign of them had to be changed accordingly. Numerical and experimental results obtained for the hydrodynamic coefficients of stern and rudder control surfaces are shown in Tables 11 and 12 respectively.

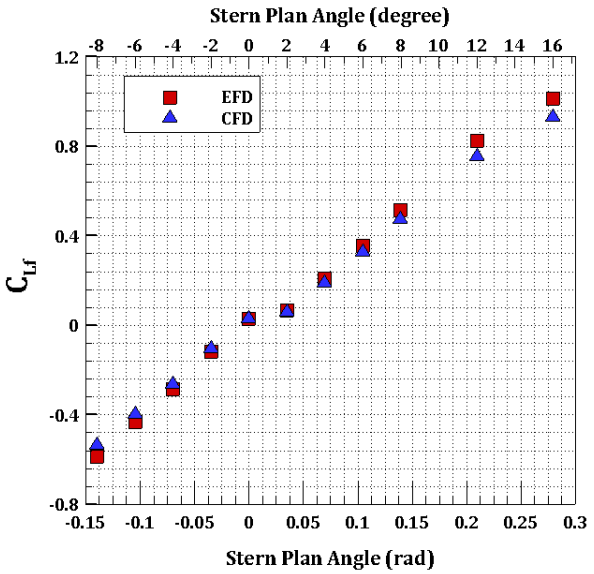

Figure 13: Variation of the fin lift coefficient with the stern angle

Table 10: Derived coefficients of the control surfaces

Hydrodynamic Coefficients	CFD	EFD	Hoerner (1985)	E (%)
$C_{Lf_{\delta_{es}}}$ (rad^{-1})	3.5045	3.8259	3.62	8.4

Table 11: Numerical and experimental results obtained for the hydrodynamic coefficients of stern control surfaces

Hydrodynamic Coefficients	CFD	EFD	Units
$Z_{uu\delta_s}$	-31.45	-34.33	kg m^{-1} rad^{-1}
$M_{uu\delta_s}$	-12.89	-14.07	kg rad^{-1}
$Z_{uw_{fin}}$	-31.45	-34.33	kg rad^{-1}
$Z_{uq_{fin}}$	-12.89	-14.07	kg rad^{-1}
$M_{uw_{fin}}$	-12.89	-14.07	kg
$M_{uq_{fin}}$	-5.29	-5.78	kg m^{-1} rad^{-1}

Table 12: Numerical and experimental results obtained for the hydrodynamic coefficients of rudder control surfaces

Hydrodynamic Coefficients	CFD	EFD	Units
$Y_{uu\delta_r}$	31.45	34.33	kg m^{-1} rad^{-1}
$N_{uu\delta_r}$	-12.89	-14.07	kg rad^{-1}
$Y_{uv_{fin}}$	-31.45	-34.33	kg rad^{-1}
$Y_{ur_{fin}}$	12.89	14.07	kg rad^{-1}
$N_{uv_{fin}}$	12.89	14.07	kg
$N_{ur_{fin}}$	-5.29	-5.78	kg m^{-1} rad^{-1}

Figure 14 illustrates local pressure contours on both sides of the stern control surface (top and bottom) in various stern angles. As can be seen, with increase in stern angle from $\delta_{es} = 4^o$ to $\delta_{es} = 16^o$, local pressure on bottom side was increased whereas it was reduced on top side of the control surface. Therefore, local pressure difference between top and bottom side of the fin was increased in +y direction, meaning that the lift force and the moment of the stern fin were increased. When stern angle decreased to negative values, local pressure on bottom side was decreased while it tended to increase on top side. Thus, local pressure difference between top and bottom side of the fin started to increase again but in the opposite direction (-y). According to streamlines illustrated in Figure 15, there is a significant flow separation on the top side of the fin at $\delta_{es} = 16^o$ due to presence of an adverse pressure gradient on the top side of the stern fin which resulted in increase of pressure drag. As this figure indicates, the reverse flow behind the control surfaces was insignificant at low stern angles.

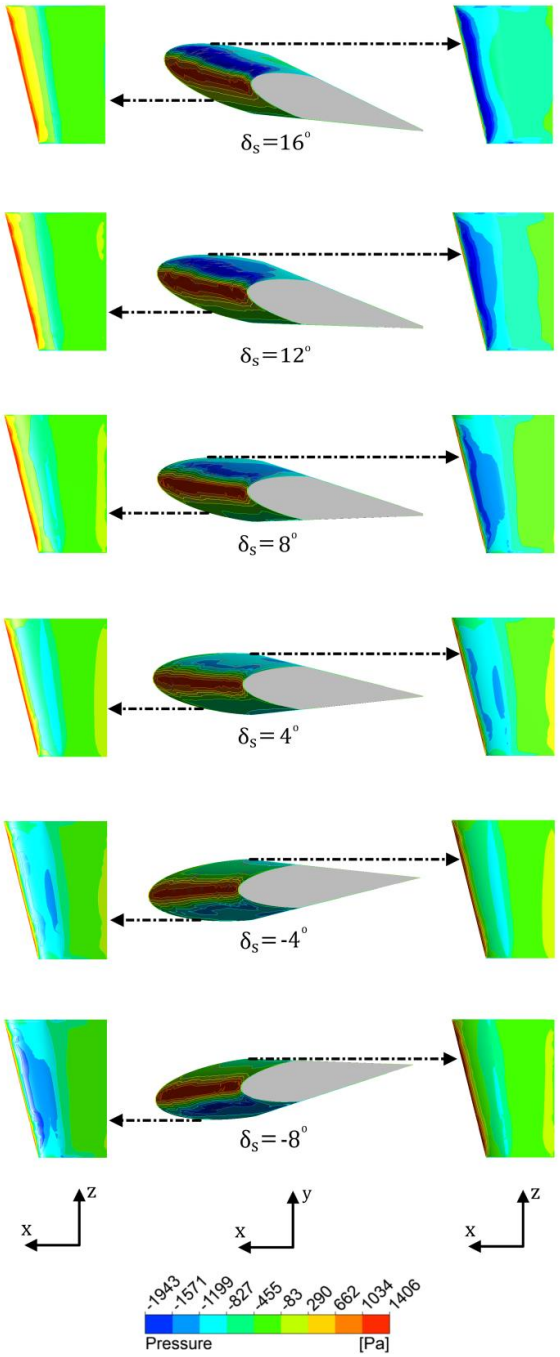

Figure 14: Variation of the local pressure on both sides (top and bottom) of the stern control surface at different stern angles

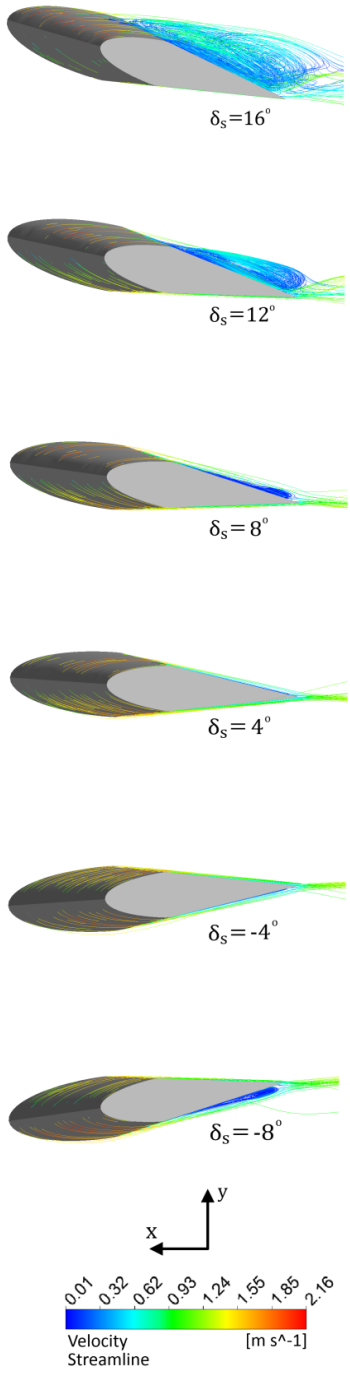

Figure 15: Variation of the velocity streamline on both sides (top and bottom) of the stern control surface at different stern angles

6. CONCLUSION

In the present study, the drag and lift related hydrodynamic coefficients of the hull and control surfaces of an AUV were calculated using both experimental and numerical methods. Experimental tests and numerical simulations were carried at various angles of attack for the hull and control surfaces. The results obtained using the current CFD model revealed that at low angles of attack, the lift and moment coefficients of the hull were in good agreement with the experimental measurements ($E < 9\%$) and the maximum difference was observed at $\alpha = 16^{o}$. This is due to the fact the free surface effect was amplified with the increasing of the hull angle of attack. Additionally, the $k-\varepsilon$ model as an eddy viscosity based turbulence model cannot capture the strength and location of the body vortex accurately at the higher angles of attack. To reduce differences between experimental and numerical results at high angles of attack employing a Reynolds Stress Model is recommended.

When it comes to the control surfaces, the resulting $C_{Lf_{\delta_{es}}}$ value obtained using CFD simulations were compared with those obtained using EFD and Hoerner (1985) correlation. It was shown that CFD results had 8.4% and 3.19% differences with EFD and Hoerner (1985) correlation respectively. Finally, the hydrodynamic coefficients obtained from the experiments agreed well with those obtained from the numerical simulations ($E = 8.4\%$). There were some differences due to the disturbances introduced by the struts connecting the AUV hull to the dynamometer in the experiments.

Streamlines behind the stern fin revealed that at $\delta_{es} = 16^{o}$, due to the presence of an adverse pressure gradient on top side of the fin, a considerable flow separation had occurred, which resulted in increasing of the pressure drag.

7. REFERENCES

1. AAGE, C. and WAGNER SMITT, L. (1994) *Hydrodynamic maneuverability data of a flatfish type AUV*. In Proceedings of the Oceans Engineering for Today's Technology and Tomorrow's Preservation, Brest, France, pp. 425-430. DOI: 10.1109/OCEANS.1994.364236.
2. ANSYS CFX, (2009) *Solver Theory Guide*. Release 12.1, ANSYS Inc., USA.
3. AVILA, J.J., NISHIMOTO, K., ADAMOWSKI, J.C. and SAMPAIO, C.M. (2012) *Experimental Investigation of the Hydrodynamic Coefficients of a Remotely Operated Vehicle Using a Planar Motion Mechanism*. Journal of Offshore Mechanics and Arctic Engineering 134. DOI: 10.1115/1.4004952.
4. BARROS, E.A.D, DANTAS, J.L.D., PASCOAL, A.M. and SA, E.D. (2008) *Investigation of Normal Force and Moment Coefficients for an AUV at Nonlinear Angle of Attack and Sideslip Range*. IEEE Journal of Oceanic Engineering 33, pp. 583-579. DOI: 10.1109/JOE.2008.2004761.
5. BELLEVRE, D., DIAZ DE TUESTA, A. and PERDON, P. (2000) *Submarine Maneuverability Assessment Using Computational Fluid Dynamic Tools*. In Proceedings of 23rd Symposium of Naval

Hydrodynamics, Val de Reuil, France, pp. 820-832.

6. BROGLIA, R., MASCIO, A.D. and AMATI, G.A. (2007) *Parallel Unsteady RANS Code for the Numerical Simulations of Free Surface Flows*. 2nd international Conference on Marine Research and Transportation, Naples, Italy.
7. CHESNAKAS, C.J. and SIMPSON, R.L. (1997) *Detailed investigation of the three-dimensional separation about a 6:1 prolate spheroid Estimation*. AIAA Journal 35, pp. 990-999. DOI: 10.2514/2.208.
8. COLEMAN, H. and STEELE, W. (1999) *Experimental and Uncertainty Analysis for Engineers*. 2nd Ed. New York, NY, John Wiley & Sons.
9. FERZIGER, J.H., PERIC, M. (2002) *Computational Methods for Fluid Dynamics*. 3rd Ed. Springer-Verlag Berlin Heidelberg New York. DOI: 10.1007/978-3-642-56026-2.
10. GERTLER, M. (1967) *The DTMB Planar-Motion-Mechanism System*, Naval Ship Research And Development Centre, Carderock, Md, Report 2528.
11. HOPKIN, D. and HERTOG, V. (1933) *The Hydrodynamic Testing and Simulation of an Autonomous Underwater Vehicle*. In Proceedings of the Second Canadian Marine Dynamics Conference, pp. 274-281.
12. HOERNER, S.F. (1965) *Fluid Dynamic Drag*. Published by author, New York City, USA.
13. HOERNER, S.F. and HENRY, V. B. (1985) *Fluid Dynamic Lift*, Published by author, 2nd Ed. New York City, USA.
14. HUMPHREYS, D. (1981) *Dynamics and hydrodynamics of ocean vehicles*. Proceedings of IEEE OCEANS'81, Boston, MA, USA, pp. 88–91. DOI:10.1109/OCEANS.1981.1151683.
15. ITTC, Recommended Procedures and Guidelines 7.5-01-01-01, 2002.
16. ITTC, Recommended Procedures and Guidelines Practical Guidelines for Ship CFD Applications 7.5-03-02-03, 2011.
17. ITTC, Uncertainty Analysis in CFD Verification and Validation 7.5-03-01-01, 2017.
18. JAGADEESH, P. and MURALI, K. (2010) *Rans predictions of free surface effects on axisymmetric underwater body*. Engineering Applications of Computational Fluid Mechanics 4, pp. 301-313. DOI: 10.1080/19942060.2010.11015318.
19. JAGADEESH, P., MURALI, K. and IDICHANDY V.G. (2009) *Experimental investigation of hydrodynamic force coefficients over AUV hull form*. Journal of Ocean Engineering 36, pp. 113-118. DOI:10.1016/j.oceaneng.2008.11.008.
20. JAVANMARD, E., *Determination of Hydrodynamic Coefficients of an AUV with Computational Fluid Dynamics and Experimental Fluid Dynamics Methods*. MSc thesis, Isfahan University of Technology, 2013.
21. JAVANMARD, E. and MANSOORZADEH, SH. (2019) *A Computational Fluid Dynamics Investigation on the Drag Coefficient Measurement of an AUV in a Towing Tank.* Journal of Applied Fluid Mechanics 12, pp. 947-959. DOI:10.29252/jafm.12.03.29525.
22. JONES, D.A., CLARKE, D.B., BRAYSHAW, I.B., BARILLON, J.L. and ANDERSON, B. (2002) *The Calculation of Hydrodynamic Coefficients for Underwater Vehicles*. Technical report DSTO Platforms Sciences Laboratory, 506 Lorimer St, Fishermans Bend, Victoria 3207, Australia.
23. KIM, H., LEONG, Z.Q., RANMUTHUGALA, D., FORREST, A. (2015) *Simulation and Validation of an AUV in Variable Accelerations*. International Journal of Offshore and Polar Engineering 25, pp. 35-44.
24. KRISHNANKUTTY, P., SUBRAMANIAN, V.A., FRANCIS, R., NAIR, P.P. and SUDARSAN, K. (2014) *Experimental and Numerical Studies on an Underwater Towed Body*. In Proceedings of the ASME 33rd International Conference on Ocean, Offshore and Arctic Engineering, San Francisco, USA. 8-13. DOI: 10.1115/OMAE2014-24400.
25. LEE, S.K., JOUNG, T.H., CHEON, S.J., JANG, T.S. and LEE, J.H. (2011) *Evaluation of the added mass for a spheroid-type unmanned underwater vehicle by vertical planar motion mechanism test*. Journal of Ocean Engineering 3, pp. 174-180. DOI: 10.2478/IJNAOE-2013-0060.
26. LEONG, Z.Q., RANMUTHUGALA, D., PENESIS, I. and NGUYEN, H. (2015) *Rans-based CFD prediction of the hydrodynamic coefficients of DARPA SUBOFF geometry in straight-line and rotating arm manoeuvres*. Transactions of the Royal Institution of Naval Architects Part A: International Journal of Maritime Engineering 157, pp. A41-A51. DOI:10.3940/rina.ijme.2015.al.308.
27. LIANG, X., LI, Y., PENG, Z., ZHANG, J. (2016) *Nonlinear dynamics modeling and performance prediction for underactuated AUV with fins*. Nonlinear Dynamics 84, pp. 237-249. DOI: 10.1007/s11071-015-2442-1.
28. MAEDA, H. and TATSUTA, S. (1989) *Prediction method of hydrodynamic stability derivatives of an autonomous non-tethered submerged vehicle*. In Proceedings of the Eighth International Conference on Offshore Mechanics and Artic Engineering, The Hague, Netherlands, pp. 105-114.
29. MALIK, S.A. and GUANG, P. (2013) *Transient Numerical Simulation for Hydrodynamic Derivatives Prediction of an Axisymmetric Submersible Vehicle*. Research Journal of

Applied Science, Engineering and Technology 5, pp. 5003-5011. DOI:10.19026/rjaset.5.4388.

30. MANSOORZADEH, SH. and JAVANMARD, E. (2014) *An investigation of free surface effects on drag and lift coefficients of an autonomous underwater vehicle (AUV) using computational and experimental fluid dynamics methods*. Journal of Fluids and Structures 51, pp. 161-171. DOI: 10.1016/j.jfluidstructs.2014.09.001.
31. NAHON, M. (1993) *Determination of undersea vehicle hydrodynamics derivatives using the USAF datcom*. In Proceedings of OCEANS '93, Victoria, Canada, pp. 283-288. DOI:10.1109/OCEANS.1993.326107.
32. PHILLIPS, A., FURLONG, M. and TURNOCK, S.R. (2007) *The use of Computational Fluid Dynamics to Determine the Dynamic Stability of an Autonomous Underwater Vehicle*. In 10th Numerical Towing Tank Symposium (NuTTS'07), Hamburg, Germany, pp. 6-11.
33. PHILLIPS, A., FURLONG, M. and TURNOCK, S.R. (2010a) *The use of computational fluid dynamics to aid cost-effective hydrodynamic design of autonomous underwater vehicles*. Proceedings of the Institution of Mechanical Engineers, Part M: Journal of Engineering for the Maritime Environment, pp. 239-254. DOI: 10.1243/14750902JEME199.
34. PHILLIPS, A., TURNOCK, S.R. and FURLONG, M. (2010b) *Influence of turbulence closure models on the vertical flow field around a submarine body undergoing steady drift*. Journal of Marine Science and Technology 15, pp. 201-217. DOI: 10.1007/s00773-010-0090-1.
35. PETERSON, R.S. (1980) *Evaluation of semi-empirical methods for predicting linear static and rotary hydrodynamic coefficients*. Technical Report, Naval Coastal Systems Center, NCSC TM-291-80, Panama City, Florida, USA.
36. POOK, D.A., CLARKE, D.B., JONES, M., QUICK H. and RANMUTHUGALA, D. (2018) *RANS based CFD Prediction of Submarine Hydrodynamic Loads*. 21st Australasian Fluid Mechanics Conference, Adelaide, Australia.
37. PRESTERO, T., *Verification of a Six-Degree of Freedom Simulation Model for the REMUS Autonomous Underwater Vehicle*. MSc thesis, Massachusetts Institute of Technology, 2001.
38. RHEE, K., YOON, H.K., SUNG, H.K., KIM, S.H. and KANG, J.N. (2001) *An Experimental Study on Hydrodynamic Coefficients of Submerged Body Using Planar Motion Mechanism and Coning Motion Device*. In International Workshop on Ship Manoeuvrability, pp. 1-20.
39. RICHARDSON, L.F. (1911) *The approximate arithmetical solution by finite difference of physical problems involving differential equations, with an application to the stresses in a masonry dam*. Philosophical Transactions of the Royal Society of London. Series A, Containing Papers of a Mathematical or Physical Character 210, pp. 459-470. DOI: 10.1098/rsta.1911.0009.
40. RICHARDSON, L.F. and GANT, J.A., (1927) *The deferred approach to the limit*. Philosophical Transactions of the Royal Society of London 226, pp. 636-646. DOI: 10.1098/rsta.1927.0008.
41. RIDLEY, P., FONTAN, J. and CORKE, P. (2003) *Submarine Dynamic Modelling*. Proceedings of the Australasian Conference on Robotics & Automation, Australian Robotics & Automation Association, Brisbane, Australia.
42. SAIEDINEZHAD, A., DEHGHAN, A.A., DEHGHAN MANSHADI, M. (2015) *Experimental investigation of hydrodynamic characteristics of a submersible vehicle model with a non-axisymmetric nose in pitch maneuver*. Journal of Ocean Engineering 100, pp. 26-34. DOI: 10.1016/j.oceaneng.2015.03.010.
43. SAKAMOTO, N. *URANS, DES Simulations of Static and Dynamic Manoeuvring for Surface Combatant*. PhD thesis, University of Iowa, 2009.
44. TANG, S., URA, T., NAKATANI, T., THORNTON, B. and JIANG, T. (2009) *Estimation of the Hydrodynamic Coefficients of the Complex-Shaped Autonomous Underwater Vehicle TUNA-SAND*. Journal of Marine Science and Technology 14, pp. 373-386. DOI: 10.1007/s00773-009-0055-4.
45. TRIANTAFYLLOU, M.S. (2002) *Manoeuvring and control of surface and underwater vehicles*. Lecture Notes for MIT Ocean Engineering Course 1, M.I.T. Cambridge, Mass, USA.
46. TYAGI, A. and SEN, D. (2006) *Calculation of transverse hydrodynamic coefficients using computational fluid dynamic approach*. Journal of Ocean Engineering 33, pp. 798-809. DOI: 10.1016/j.oceaneng.2005.06.004.
47. WU, B.S., FU, X., KUANG, X.F. and MIAO, Q.M. (2005) *Investigation of Hydrodynamic Characteristics of Submarine Moving Close to the Sea Bottom with CFD Methods*. Journal of Ship Mechanics 73, pp.19-28.
48. WHITE, F.M. (1985) *Fluid Mechanics*. 4th Ed. University of Rhode Island, Narragansett.
49. WHITE, F.M. (2006) *Viscous Fluid Flow*. 3rd Ed. University of Rhode Island, Kingston, USA.
50. WILSON, R.V., STERN, F., COLEMAN, H.W. and PATRSON E.G. (2001) *Comprehensive approach to verification and validation of CFD simulations − part 2: application for RANS simulation of a Cargo/Container ship*. J. Fluids Eng. 123, pp. 803–810. DOI: 10.1115/1.1412236.
51. ZHANG, H., XU, Y.R. and CAI, H.P. (2010) *Using CFD Software to Calculate*

Hydrodynamic Coefficients. Journal of Marine Science and Application 9, pp.149-15. DOI: 10.1007/s11804-010-9009-9.

52. ZHANG, X.G. and ZOU, Z.J. (2013). *Estimation of the hydrodynamic coefficients from captive mode test results by using support vector machines*. Journal of Ocean Engineering 73, pp. 25-31. DOI: 10.1016/j.oceaneng.2013.07.007.

